Supplementary Information for:

Novel butterfly-shaped organic semiconductors and single-walled carbon nanotubes composites for high performance thermoelectric generator

Lai Wei,[1, 2] Hongfeng Huang,[1] Chunmei Gao,[3] Danqing Liu,*[1] Lei Wang*[1, 2]

[1]Shenzhen key Laboratory of Polymer Science and Technology, College of Materials Science and Engineering, Shenzhen University, Shenzhen, 518060, China
[2]Key Laboratory of Optoelectronic Devices and Systems of Ministry of Education and Guangdong Province, college of Optoelectronic Engineering, Shenzhen University, Shenzhen 518060, China
[3] College of Chemistry and Environmental Engineering, Shenzhen University, Shenzhen 518060, China

Contents：

1. Materials

All starting compounds were purchased from Energy Chemical Co., Ltd. and used without further treatment unless otherwise noted. SWCNTs (diameter: 1–2 nm, purity: >95.0 wt%) were purchased from XFNANO Materials Technology Co., Ltd (Nanjing, China). Anhydrous chlorobenzene was purchased from Sun Chemical Technology Co., Ltd (Shanghai). The raw materials including n-BuLi, pentacenone were purchased from Sun Chemical Technology Co., Ltd (Shanghai). Other chemical reagents, including ethanol, dichloromethane, acetone and isopropanol, were used as received without further treatment. Compound **1-4** and **5** were synthesized following the reported procedures and purified by silica gel column chromatography (eluent: CH_2Cl_2: hexane = 2:1) and then recrystallized from ethyl acetate.

2. Synthesis

General: The reagents and starting materials employed were commercially available and used without any further purification if not specified elsewhere. Anhydrous and oxygen-free THF and CH_2Cl_2 were purified by an Advanced Technology Pure-Solv PS-MD-4 system. ^{1}H NMR (500 MHz) or ^{13}C NMR (100 MHz) spectra were recorded on a Brucker ADVANCE III spectrometer.

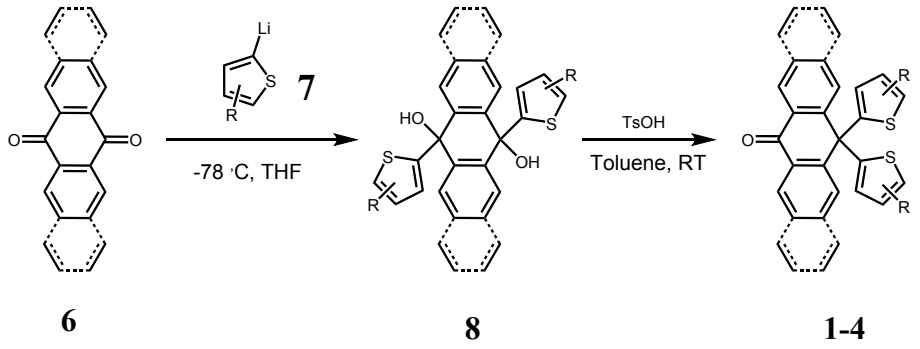

Scheme S1 Synthesis of butterfly-shaped pentacenone derivatives **1-4**

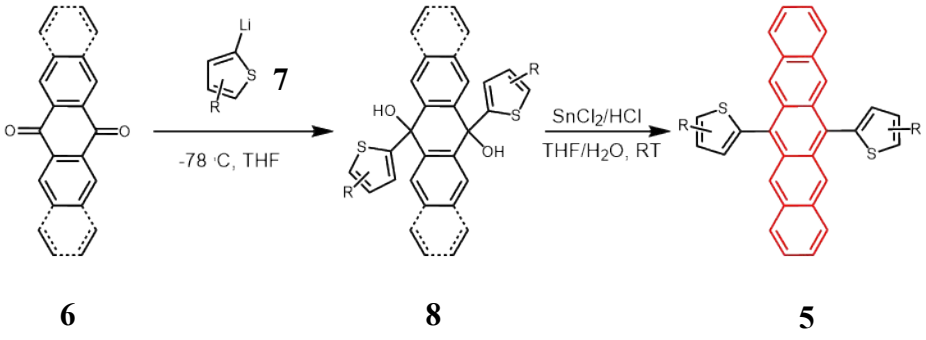

Scheme S2 Synthesis of planar pentacenone derivatives **5**

Procedure A：Compounds **8** were synthesized according to the literature[1].

Procedure B: Under N2 atmosphere compounds **8** (0.798 mmol, 1 eq.) was added into a mixture of TsOH (0.798 mmol, 1 eq.) in dry Toluene (33 mL). The mixture was stirred overnight until the substrates was totally consumed. After that, the solvent was evaporated and the residue was purified by chromatography with PE/DCM 1/1 to afford **1-4** as a yellow solid.

Procedure C: Compound **5** was synthesized according to the literature[2].

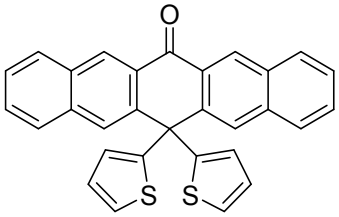

13,13-di(thiophen-2-yl) pentacen-6(13H)-one (**1**)

Yellow solid, yield 42%.

^{1}H NMR (500 MHz, DMSO-d6) δ 8.88 (s, 2 H), 8.27 (d, *J* = 7.5 Hz, 2 H), 7.99 (d, *J* = 8.0 Hz, 2 H), 7.83 (s, 2 H), 7.72-7.64 (m, 4 H), 7.54 (dd, *J* = 5.5 & 1.5 Hz, 2 H), 7.00 (dd, *J* = 5.0 & 3.5 Hz, 2 H), 6.67 (dd, *J* = 3.5 & 1.0 Hz, 2 H).

^{13}C NMR (125 MHz, DMSO) δ 151.9, 151.4, 143.3, 134.7, 131.7, 129.7, 129.4, 129.2, 129.1, 128.8, 128.2, 128.2, 127.6, 127.3, 126.7, 115.2.

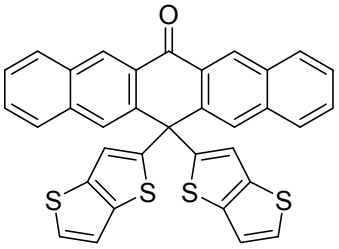

13,13-bis(thieno[3,2-b]thiophen-2-yl) pentacen-6(13H)-one (**2**)

Yellow solid, 40 % yield.

^{1}H NMR (500 MHz, CDCl3) δ 9.16 (s, 2 H), 8.10 (s, 2 H), 7.65-7.59 (m, 2 H), 7.25-7.20 (m, 4 H), 7.14-7.09 (m, 2 H), 6.86 (s, 2 H), 6.77 (d, *J* = 5.5 Hz, 2 H), 6.65 (d, *J* = 5.5 Hz, 2 H).

^{13}C NMR (125 MHz, $CDCl_3$) δ 183.6 (C), 154.3, 143.1, 140.6, 138.2, 135.5, 132.9, 130.7, 130.5, 130.0, 129.2, 128.8, 128.6, 128.4, 128.2, 128.0, 127.6, 127.4, 122.0, 119.7.

---

1 R. Sekiya, K. Kiyo-oka, T. Imakubo, K. Kobayashi, *J. Am. Chem. Soc.*, 2000, **122**, 10282-10288.

2 J. Wang, K. Liu, Y.-Y. Liu, C.-L. Song, Z.-F. Shi, J.-B. Peng, H.-L. Zhang, X.-P. Cao, *Org. Lett.*, 2009, **11**, 2563-2566.

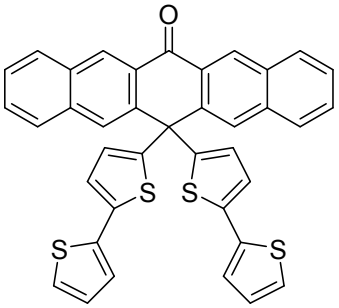

13,13-di([2,2'-bithiophen]-5-yl) pentacen-6(13H)-one (**3**)

Yellow solid, 32 % yield.

^{1}H NMR (500 MHz, $CDCl_3$) δ 8.92 (s, 2 H), 8.09 (d, *J*= 4.0 Hz, 2 H), 7.95 (s, 2 H), 7.90 (d, *J* = 4.0 Hz, 2 H), 7.69-7.51 (m, 4 H), 7.17 (d, *J*= 4.0 Hz, 2 H), 7.07-6.89 (m, 6 H), 6.59 (d, *J* = 4.0 Hz, 2 H).

^{13}C NMR (125 MHz, $CDCl_3$) δ 185.0, 150.6, 143.2, 138.9, 137.4, 135.6, 132.6, 130.24, 130.22, 130.09, 130.05, 129.2, 128.8, 128.1, 127.6, 124.9, 124.2, 122.9, 53.5.

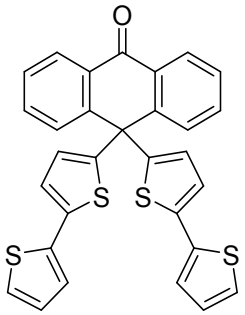

10,10-di([2,2'-bithiophen]-5-yl)anthracen-9(10H)-one (**4**)

Yelow solid, 56 % yield.

^{1}H NMR (500 MHz, $CDCl_3$) δ 8.33 (dd, *J* = 7.8&1.3 Hz, 1H), 7.64–7.60 (m, 2 H), 7.59–7.55 (m, 2H), 7.55-7.50 (m, 2 H), 7.17 (dd, *J* = 5.1&0.9 Hz, 2 H), 7.04 (dd, *J* = 3.6& 0.9 Hz, 2 H), 6.98-6.93 (m, 2 H), 6.67 (d, *J* = 3.8 Hz, 2 H).

^{13}C NMR (125 MHz, $CDCl_3$) δ 183.8, 149.8, 147.7, 138.6, 137.2, 133.5, 131.3, 130.1, 129.6, 128.6, 128.1, 128.0, 125.0, 124.2, 122.8, 52.6.

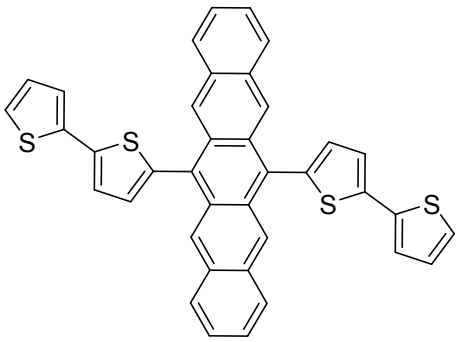

6,13-di([2,2'-bithiophen]-5-yl)pentacene (**5**)

^{1}H NMR (600 MHz, Bezene-D6) δ 9.18 (s, 2 H), 8.15 (s, 2 H), 7.64-7.61 (m, 2 H), 7.35-7.31 (m, 2 H), 7.14-7.09 (m, 4 H), 6.84 (d, *J* = 6.0 Hz, 2 H), 6.70 (dd, *J* = 3.6&1.1 Hz, 2 H), 6.62 (dd, *J* = 5.1&1.1 Hz, 2 H), 6.58 (d, *J* = 3.8 Hz, 1 H), 6.50 (dd, *J* = 5.1&3.7 Hz, 2 H).
^{13}C NMR (75 MHz, $CDCl_3$) δ 183.5, 150.8, 143.1, 138.7, 136.9, 135.2, 132.5, 130.5, 130.1, 129.8, 129.6, 128.50, 128.46, 128.2, 128.0, 127.8, 127.6, 127.0, 124.4, 124.0, 122.8, 53.5.

3. Characterization of the OSCs (1-5)

Thermogravimetry (TG) analysis were carried out to investigated the effects of the various central cores and wing-shaped substituents of these OSC on thermal properties. To investigate the thermal stability of these hybrid films, the thermal properties of the OSC were evaluated by TGA. Figure S1 revealed that the values (defined as the 5% weight loss) of OSCs (**1-5**) were 263, 137, 237, 302, 179 °C, respectively, in which butterfly-shaped molecular **2** (137 °C) bearing more bulky thieno[3,2-b]thiophene rings and the planar molecule **5** (179 °C) showed less thermal stabilities, and molecules **1**, **3**, **4** revealed excellent thermal stability, especially molecule **3** with about 50% of the weight left even at a high temperature of 400 °C. Overall, all the five materials manifested good thermal stability, which indicates that they would be promising candidates for further applications for the TE device.

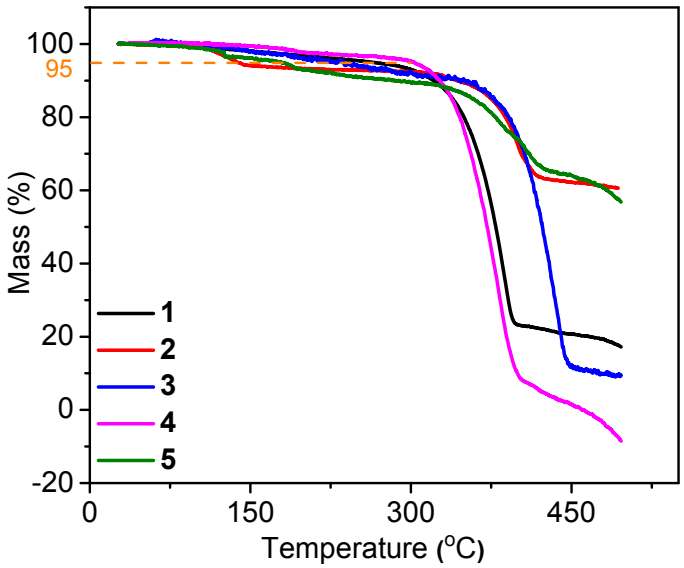

Fig. S1 TGA analysis of **1-5**

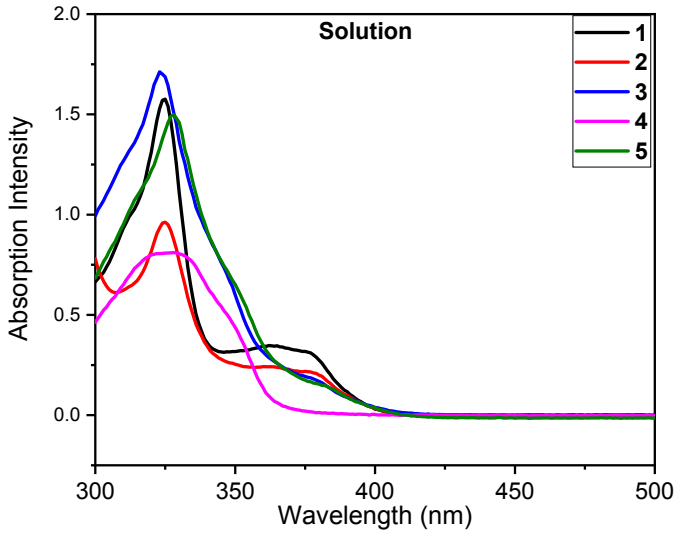

Fig. S2 UV absorption spectra of **1-5** in ClC_6H_5 ($c = 1.0\times10^{-4}$ mol/L)

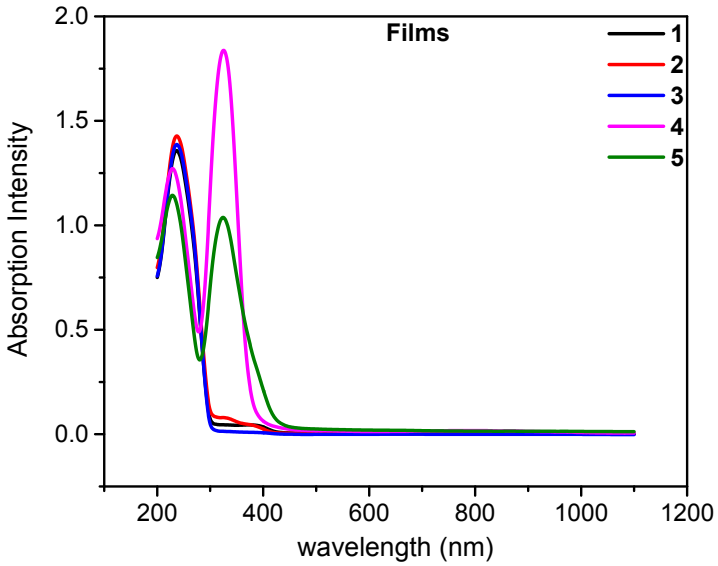

Fig. S3 UV absorption spectra of **1-5** as thin films

4. Formation and characterization of OSC/SWCNT composite films

Preparation of OSCs/SWCNT composite films:

SWCNTs are dispersed in anhydrous chlorobenzene at a concentration of 1 mg mL^{-1} using an ultrasonic cleaning machine for 4 h at room temperature, and then stirred vigorously for 24 h by using a magnetic stirrer. Next, the OSCs (**1-5**) solid powders are added into the SWCNT

dispersion to generate OSC/SWCNT mixed solution in which the concentrations of SWCNTs are 1 mg mL^{-1}. The mixture is then sonicated for 60 min to ensure thorough mixing. Glass slides (10 mm × 10 mm) are washed sequentially with dichloromethane, acetone, isopropanol and ethanol. The composite films of OSC/SWCNT are prepared by drop-casting 130 μL mixed solution on cleaned glass substrates under ambient conditions until the solvents evaporated completely.

Thermoelectric performance measurement of OSCs/SWCNT composite films：

The electrical conductivity and Seebeck coefficient of the composite films are simultaneously measured using a TE parameter test system (MRS-3, JiaYiTong Company). The composite thin films were fixed between two copper plates. The Seebeck coefficients were obtained by changing the temperature between the two copper plates, and the electrical resistivities were acquired simultaneously. The exact thicknesses of drop-cast films were measured with Microfigure measuring instrument (Surfcorder ET4000M). The obtained films have similar thickness of approximately 1.5 ~ 2.0 μm with the measured standard deviation of 0.11 ~ 0.15 μm, indicating relatively uniform surfaces. The detailed measuring process of film thickness was described as follows: Firstly, using ethanol to wipe off part of the composite films for making clear steps between the glass substrate and the rest of composite films. Then, the probe of microfigure measuring instrument scan the surface which ranges from the glass substrate to the rest of composite films. Finally, three thickness data of composite films can be obtained by the analysis software accurately. Repeat the mentioned operation above and obtain nine values totally. The final results of thickness were obtained by averaging nine thickness values.

Table S1 Thermoelectric parameters of these samples OSC (**1-5**)/SWCNT composite films

Composite films	Electrical conductivity ($S.cm^{-1}$)		Seebeck coefficient ($\mu V\ K^{-1}$)		Power factor ($\mu W\ m^{-1}\ K^{-2}$)	
	Average	Max.	Average	Max.	Average	Max.
SWCNT/**1**[a]	639.8(±62.4)	703.2	57.3(±1.00)	58.3	209.4(±7.19)	216.6
SWCNT/**2**[a]	1014.4(±7.1)	1021.5	52.2(±1.16)	53.4	276.8(±10.96)	287.8
SWCNT/**3**[a]	823.9(±82.1)	906.0	59.3(±2.01)	61.3	304.9(±6.96)	311.8
SWCNT/**4**[b]	1156.3(±33.3)	1189.6	47.1(±1.45)	48.5	238.2(±0.49)	238.6
SWCNT/**5**[a]	691.8(±5.7)	697.5	41.8(±2.51)	44.3	118.8(±16.03)	134.8

[a] With an optimized doping ratio of SWCNT/OSCs (1:1). [b] With an optimized doping ratio of SWCNT/OSC (2:1).

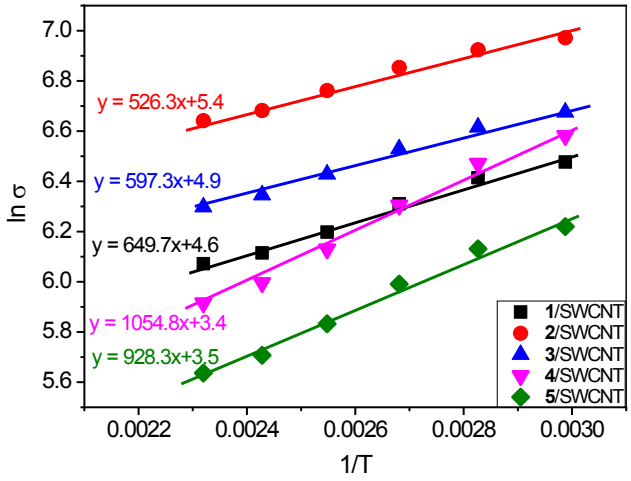

Fig. S4 Fitting of lnσ to 1/T according to metal conduction mode: $\sigma(T) = \sigma_0 exp(\hbar\omega_0/k_BT)$, where $\hbar\omega_0$ is the energy of the $2k_F$ phonons.

5. Characterization of composite films

Thermogravimetry (TG) analysis were carried out to investigate the effects of the various central cores and wing-shaped substituents of these OSC on thermal properties. To investigate the thermal stability of these hybrid films, the thermal properties of the OSC/SWCNTs were evaluated by TGA. Figure S5 revealed that the values (defined as the 5% weight loss) of OSCs (**1**-**5**)/SWCNTs were 190, 175, 296, 210, 230 °C, respectively, in which butterfly-shaped molecular **2** /SWCNT composite films (175 °C) bearing more bulky thieno[3,2-b]thiophene rings showed less thermal stabilities, and molecules **3**/SWCNT cpmposite films revealed excellent thermal stability, with about 80% of the weight left even at a high temperature of 495 °C. Overall, all the five materials manifested good thermal stability, which indicates that they would be promising candidates for further applications in the TE device field.

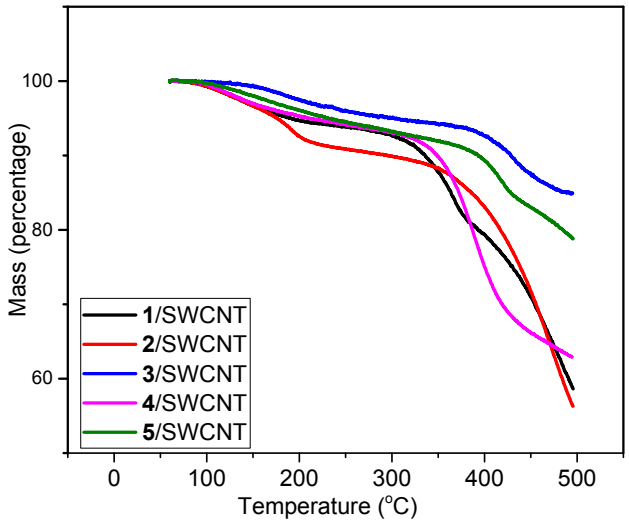

Fig. S5 TGA analysis of **1**-**5**/SWCNTs composite films

The morphologies of composite films were characterized by scan electron microscopy (SEM, HitachiS-4700, Japan). The composite films with 50% OSC loading exhibit smooth surface with three-dimensional continuous network of SWCNT bundles (Figure S6). No obvious aggregates of the small molecular OSC are observed in the SEM image indicating well dispersion of OSC molecules in the SWCNT networks due to strong π-π interactions.

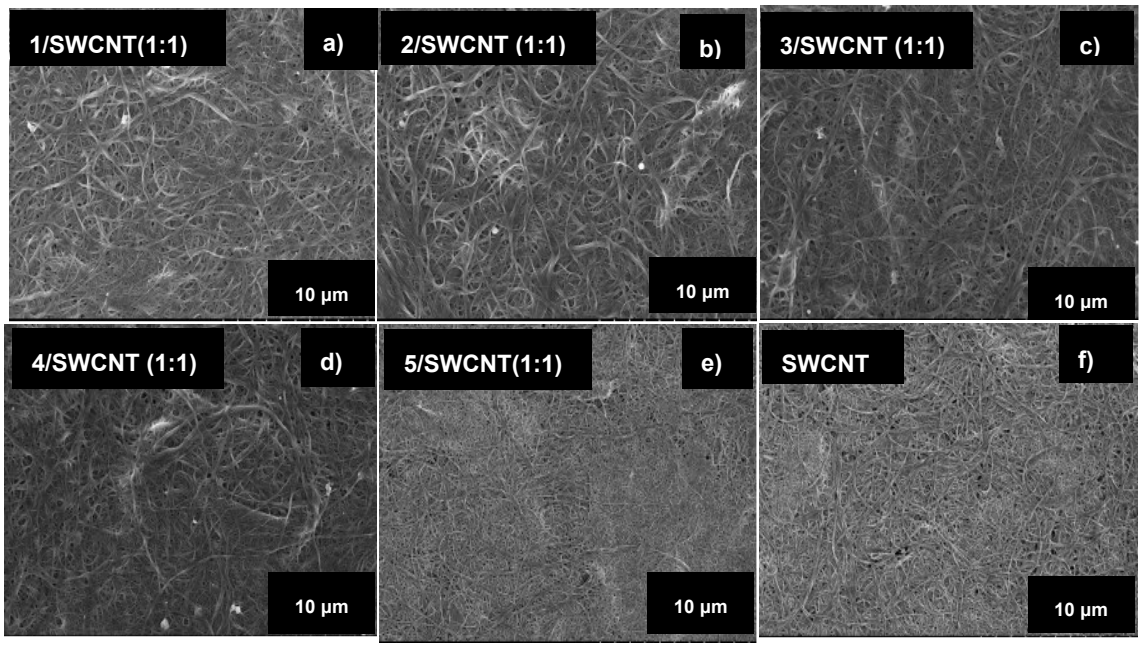

Fig. S6. SEM images of OSC/SWCNT composites. a)-h) OSC (**1**-**5**)/SWCNT with the same hybrid ratio of 1:1 and pure SWCNTs, respectively

The crystallinity of the composite films is studied by XRD. X-ray diffraction (XRD) measurements are recorded using a SmartLab X-ray diffractometer with Cu Kα radiation. The pristine and doped SWCNT films all exhibited diffraction peaks at 2θ = 26.6° and 33.6°, which corresponded to the graphite reflection (Figure S7).

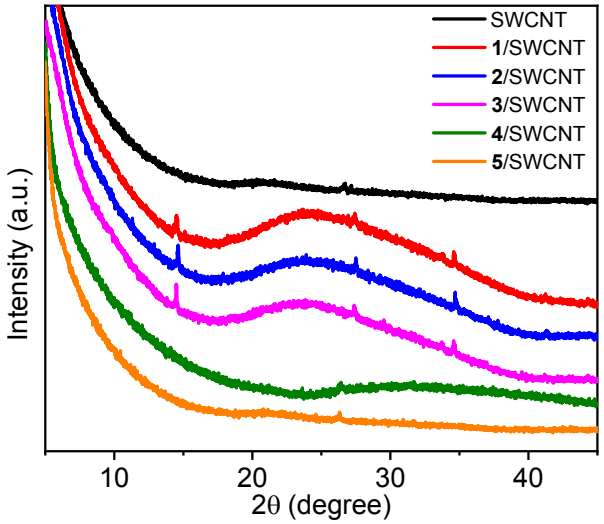

Fig. S7 XRD patterns of OSC (**1-5**)/ SWCNT composite films at 50 % OSC loading.

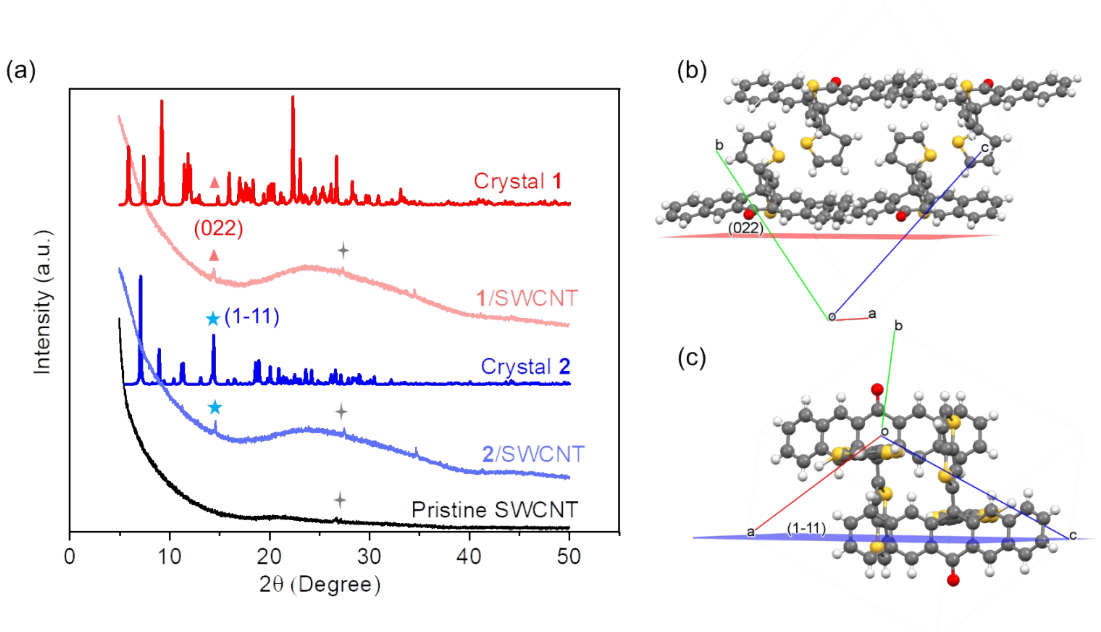

Fig. S8 (a) X-ray diffractions from single crystals of **1**, **2**, OSC/ SWCNT composite films (50% OSC loading) and pristine SWCNT film. (b) Packing structure of **1** showing the base vectors for a lattice cell and the (022) plane. (c) Packing structure of **2** showing the base vectors for a lattice cell and the (1-11) plane.

The cycling stability of the composite films based on butterfly-shaped OSCs (**2**, **3**) were tested and compared with the planar OSC **5**/SWCNTfor 2-3 cycles from 310 K to 430 K. The results indicate that the butterfly-shaped OSC (**2** and **3**) composite films had better cycling stabilities than that of planar OSC **5**/SWCNT. The composite film of **3**/SWCNT show higher cyclic stability than **2**/SWCNT, which is mainly due to its higher thermal stability as shown in the TGA analysis (Fig. S5). Especially, **3**/SWCNT composite film has more stable thermoelectric properties with only an 8 % reduction of PF value at 310 K from 299.9 μW m^{-1} K^{-2} to 276.8 μW m^{-1} K^{-2} for 3 cycles. In contrast, the PF value of planar OSC **5**/SWCNT at 310 K exhibited an 27% reduction due to a 32% reduction on electrical conductivities in the second cycle. This result indicate that the composite films based on butterfly-shaped OSCs show higher cyclic stability than **5**/SWCNT composite film, which is probably because of their more stable electrical conductivities through enhancing the interactions between butterfly-shaped molecules and SWCNT.

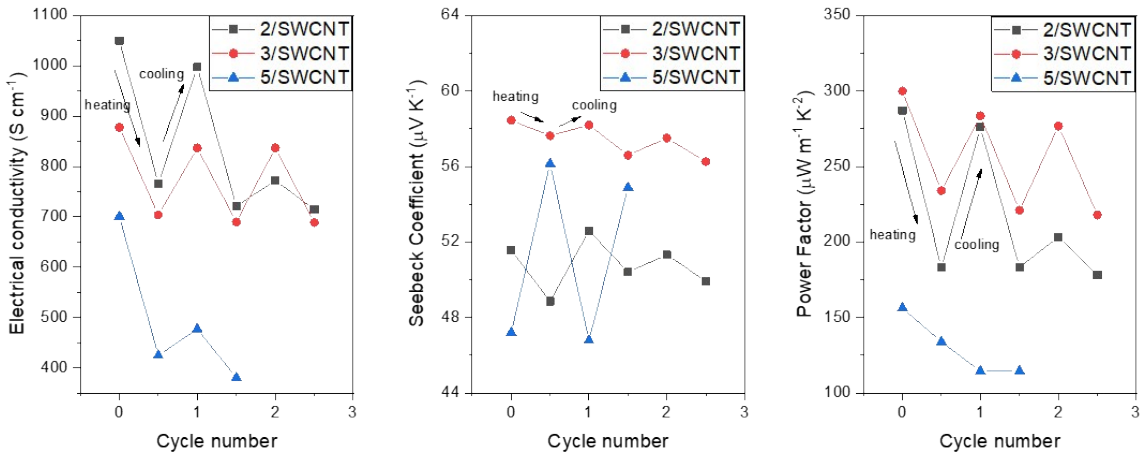

Fig. S9 Thermoelectric properties of three OSCs/SWCNT composite films with heating and cooling for three cycles from 310 K to 430 K.

6. Preparation and measurement of the TEG performance of composite films

Preparation of OSCs/SWCNT thermoelectric modules：

Flexible organic thermoelectric generators (TEGs) composed of 10 active p-type OSC doped SWCNT films were fabricated by drop-casting on a uniform polyimide substrate. All the composite films are cut into rectangular strips with dimensions of 2 cm (length) × 7 mm (width) × 4 μm (thickness). Then, the composite films are connected in series with silver paste and copper glue. Subsequently, copper foils were attached to both ends of the device with silver paste to contact the probe to detect the performance by a probe station.

Measurement of OSCs/SWCNT thermoelectric modules：

The TE performances of flexible modules including the voltage–current curve and power–current curve are tested using a Keithley 4200-SCS system under ambient air, and the temperatures are monitored by thermocouples (TC-OMEGA).

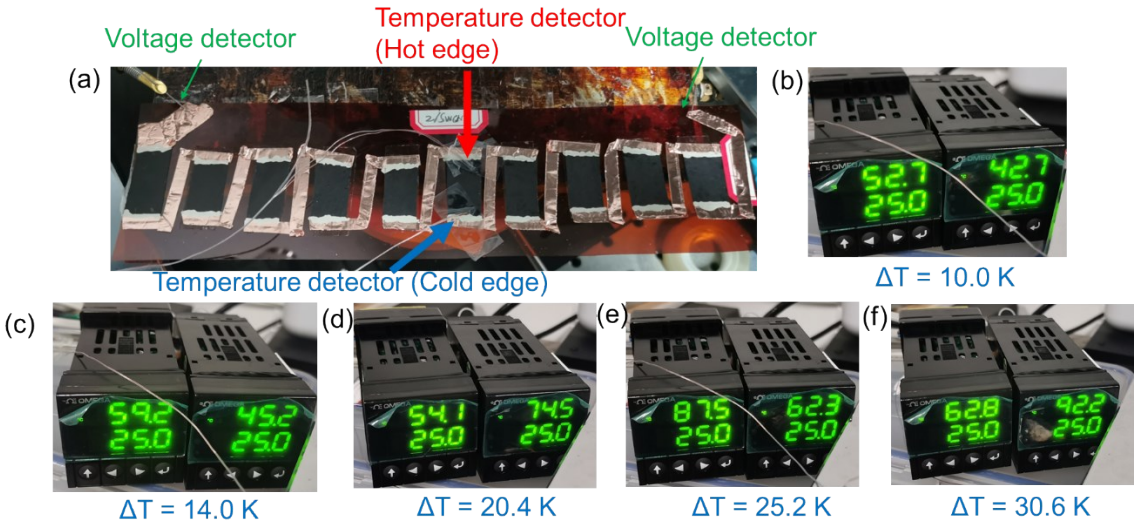

Fig. S10 Photos of TEG modules; (a)-(f): Photos of temperature detection with different ΔT monitored by thermocouples.

Table S2 Summary of TEG performances

ΔT	**1**/SWCNT		**2**/SWCNT		**3**/SWCNT		**4**/SWCNT		**5**/SWCNT	
	V_{oc} (mV)	Power (μW)	V_{oc} (mV)	Power (μW)	V_{oc} (mV)	Power (μW)	V_{oc} (mV)	Power (μW)	V_{oc} (mV)	Power (μW)
10K	4.15±0.39	0.17±0.04	6.06±0.46	0.28±0.06	5.60±0.14	0.33±0.01	3.47+0.18	0.14±0.01	3.13±0.19	0.10±0.01
14K	6.11±0.49	0.40±0.04	8.36±0.11	0.54±0.01	7.44±0.15	0.51±0.04	5.36+0.29	0.33±0.02	4.55±0.20	0.21±0.02
20K	8.27±0.20	0.73±0.01	11.41±0.62	1.00±0.10	10.10±0.38	1.07±0.08	7.05+0.10	0.57±0.02	6.84±0.27	0.48±0.04
25K	10.03±0.19	1.02±0.04	13.53±0.50	1.50±0.07	12.20±0.08	1.41±0.14	9.21+0.45	0.93±0.08	9.10±0.32	0.81±0.05
31K	12.61±0.53	1.63±0.14	16.60±0.03	2.07±0.01	13.28±0.81	1.85±0.07	11.76+0.26	1.44±0.03	11.35±0.31	1.21±0.05

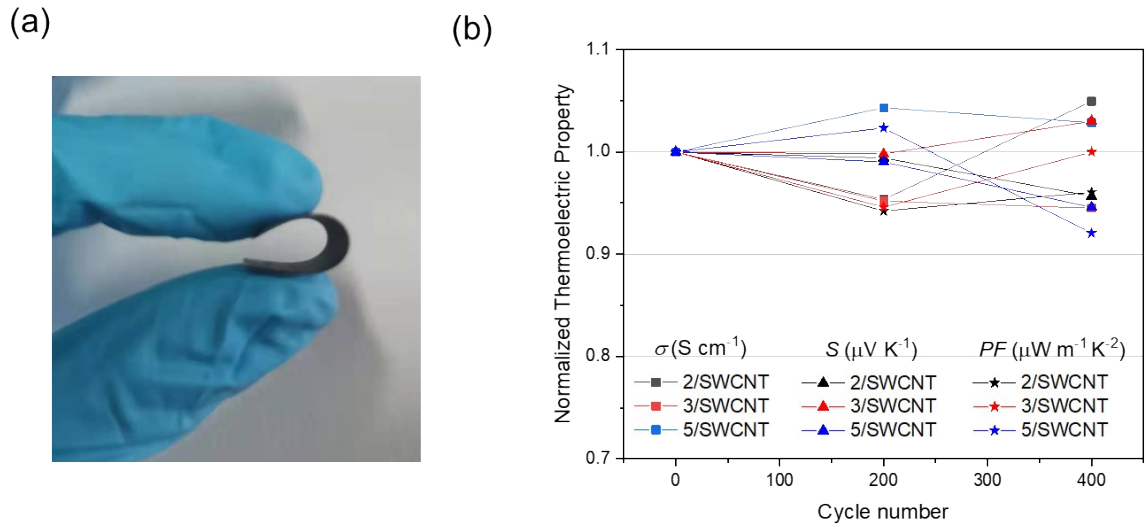

Fig. S11 (a) Photo of flexible films. (b) The normalized thermoelectrical properties (σ, S and PF) of three composite films at different bending times.

Table S3 Flexibilities of the pristine SWCNT and OSCs/SWCNT composite films on polyimide substrate with 50% OSC loading.

Times of Bending	0			200			400		
Film name	σ (S.c m^{-1})	*S* (μV K^{-1})	PF (μW m^{-1} K^{-2})	σ (S.c m^{-1})	*S* (μV K^{-1})	PF (μW m^{-1} K^{-2})	σ (S.c m^{-1})	*S* (μV K^{-1})	PF (μW m^{-1} K^{-2})
2/SWCNT	1053.2	52.21	287.1	1004.3	51.90	270.5	1105.2	49.95	275.8
3/SWCNT	844.4	59.92	303.2	803.3	59.76	286.9	797.5	61.78	303.3
5/SWCNT	527.7	45.03	107.0	550.5	44.59	109.5	542.8	42.59	98.5
SWCNT	1422.7	28.72	117.4	1475.3	27.80	114.0	1334.8	26.62	94.6

We also compared the measured output voltages (V_m) of TEGs with the theoretical voltages (V_{th}) as shown in Fig. S12. The V_{th} is calculated by $V_{th} = NS\Delta T$, where N is the number TE legs, and *S* is Seebeck coefficients for the composite films. It was founded that the V_m has a good linear relationship with the increase of ΔT and is slightly lower to the V_{th}. This can be attributed to two aspects. Firstly, the film microstructures might be different due to different surface properties of the substrates. Secondly, the contact resistance and energy lost existed in the TEGs, which was widely observed in TEGs solely fabricated by p-type components (J. Mater. Sci-Mater. El., 2019, 30, 20369**;** Chem. Eng. J., 2020, 381, 122650).

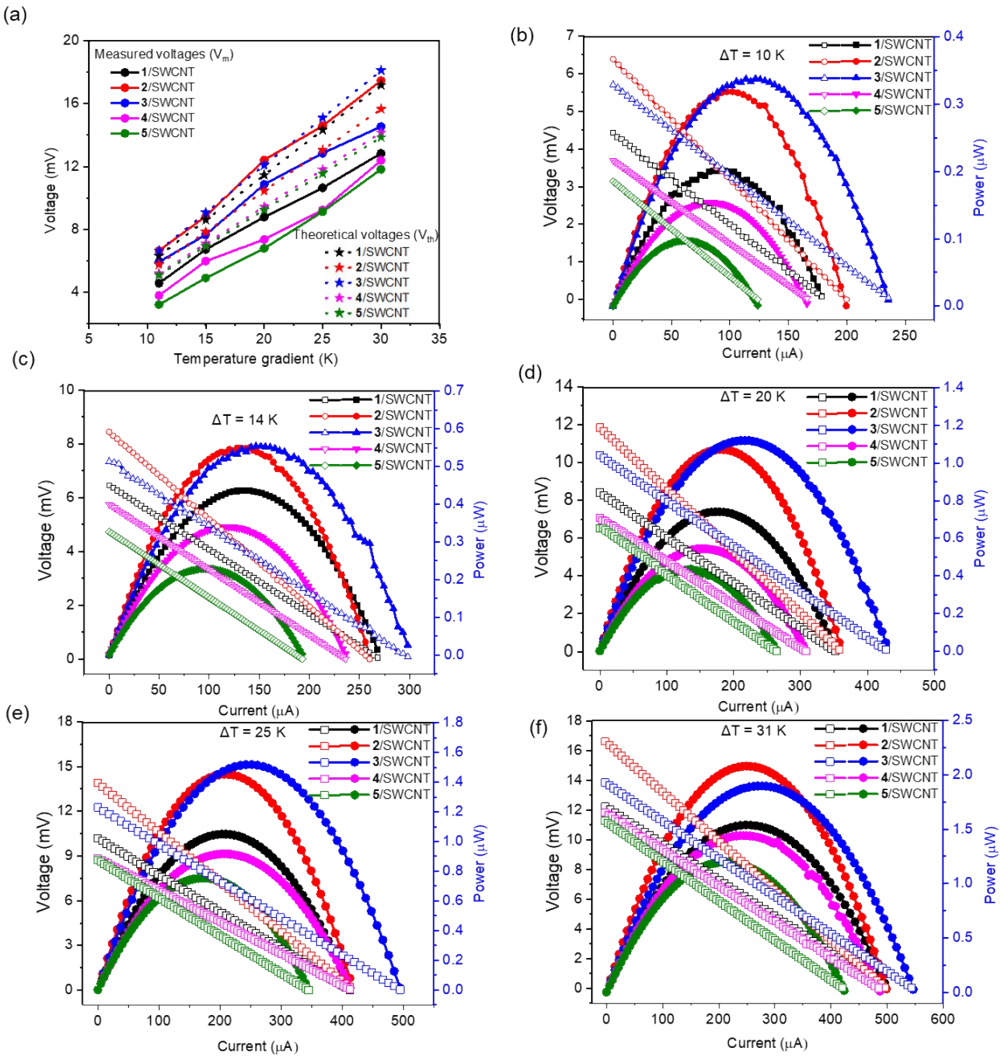

Fig. S12 (a) Theoretical (V_{th}) and measured (V_m) open-circut voltage dependence of temperature gradient. (b)-(f) Power-current output (solid circles) and voltage-current output curves (open squares) for five TE modules at temperature gradients.

7. NMR spectra

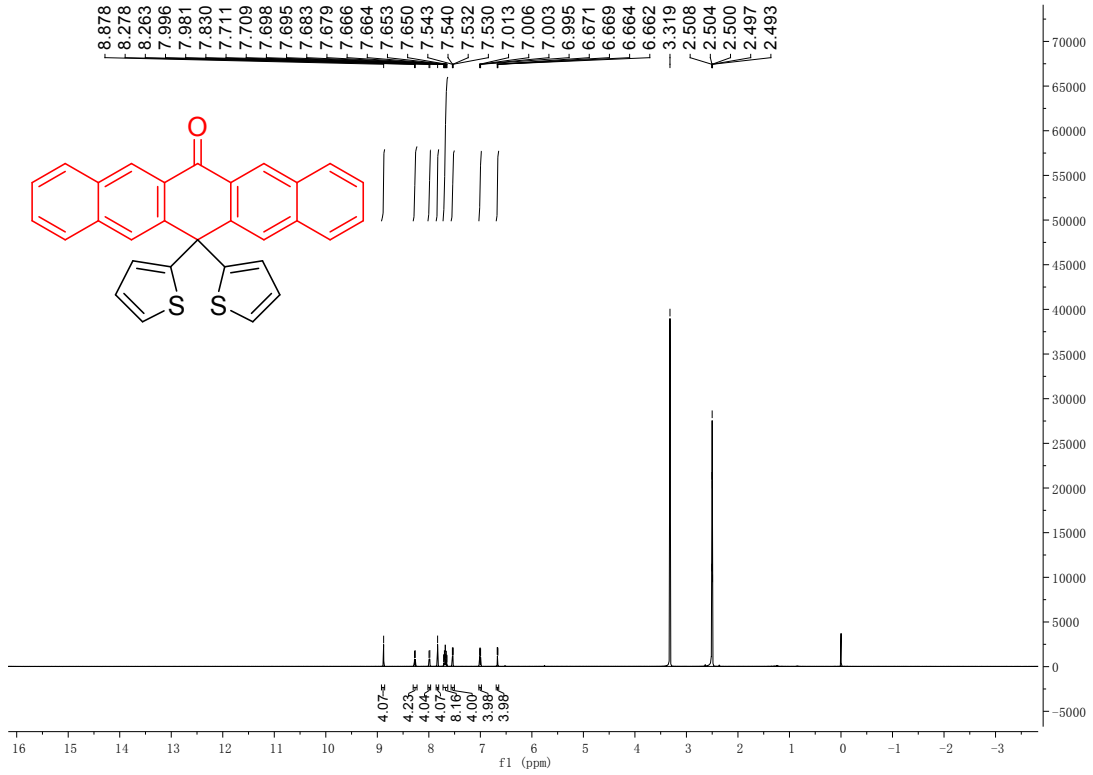

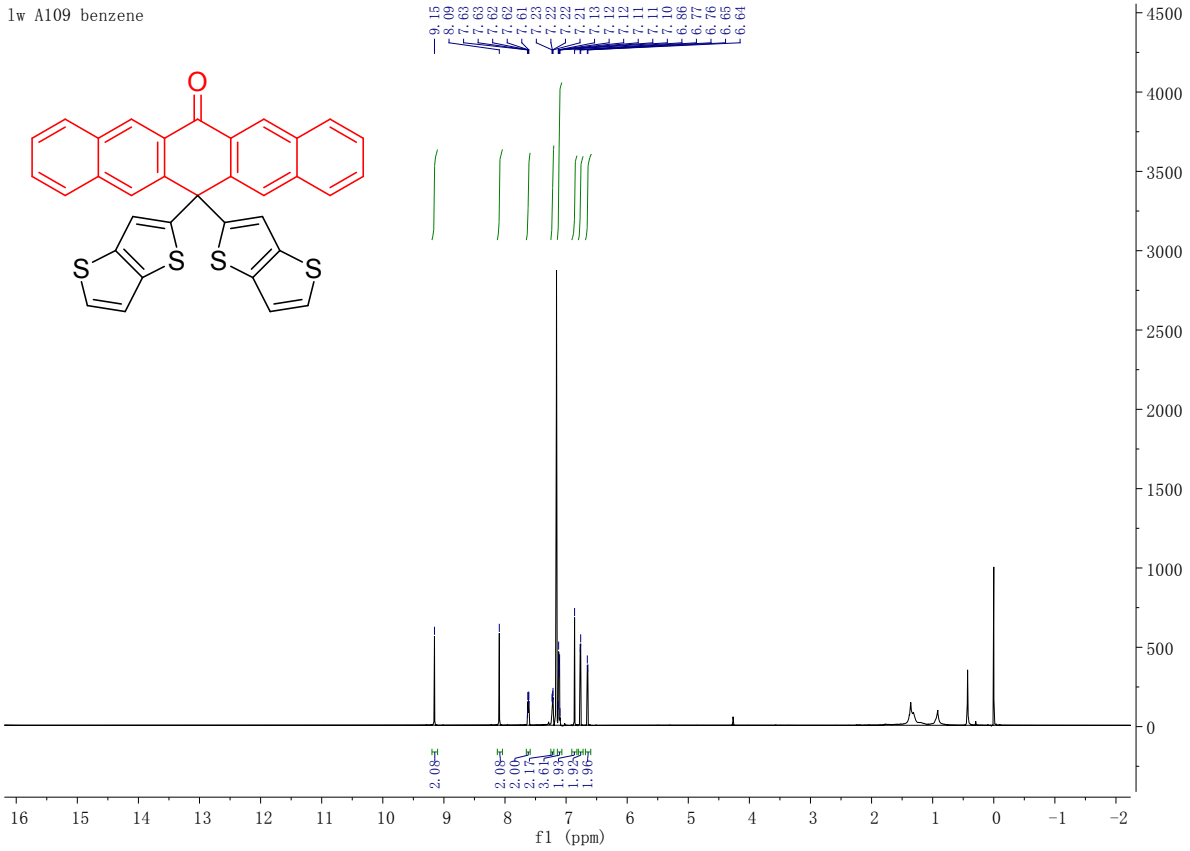

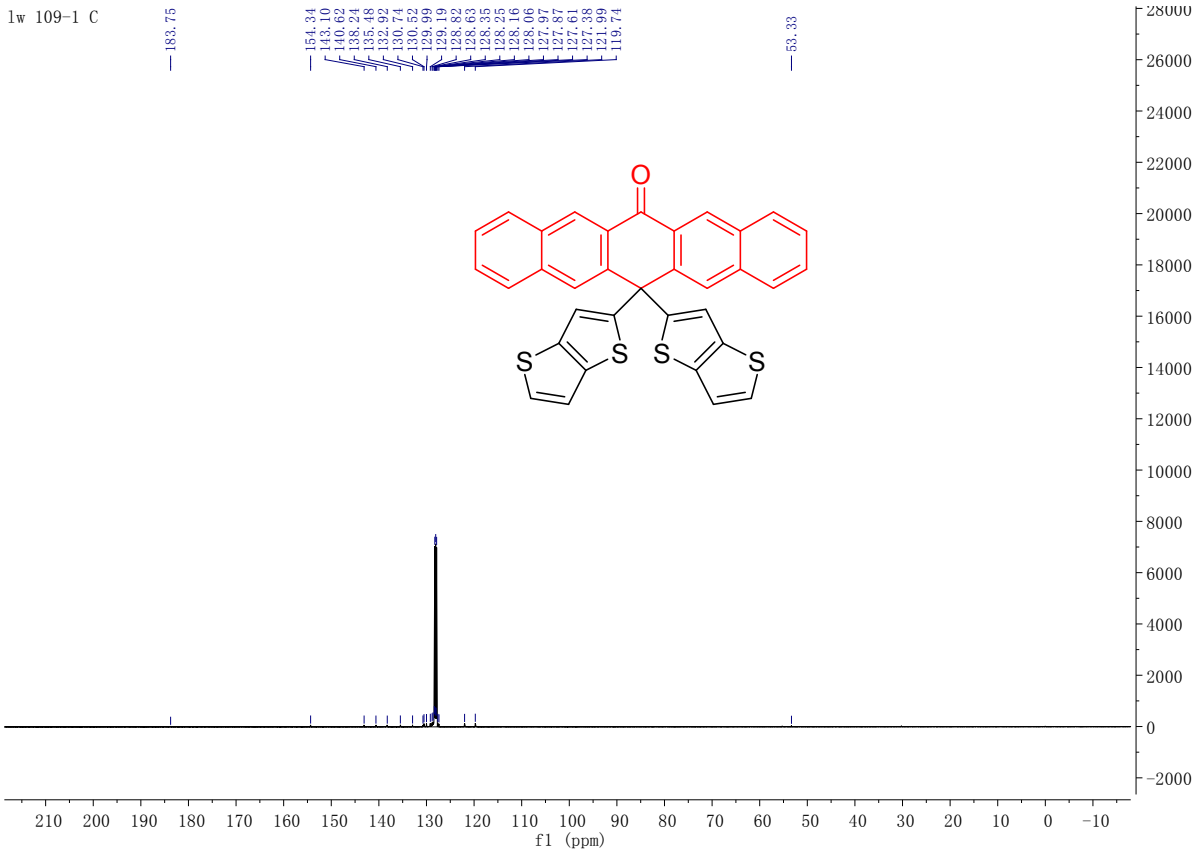
lw 109-1 C
183.75
154.34
143.10
140.62
138.24
135.48
132.92
130.74
130.52
129.99
129.19
128.82
128.63
128.35
128.25
128.16
128.06
127.97
127.87
127.61
127.38
121.99
119.74
53.33
O
S
S
S
S
f1 (ppm)

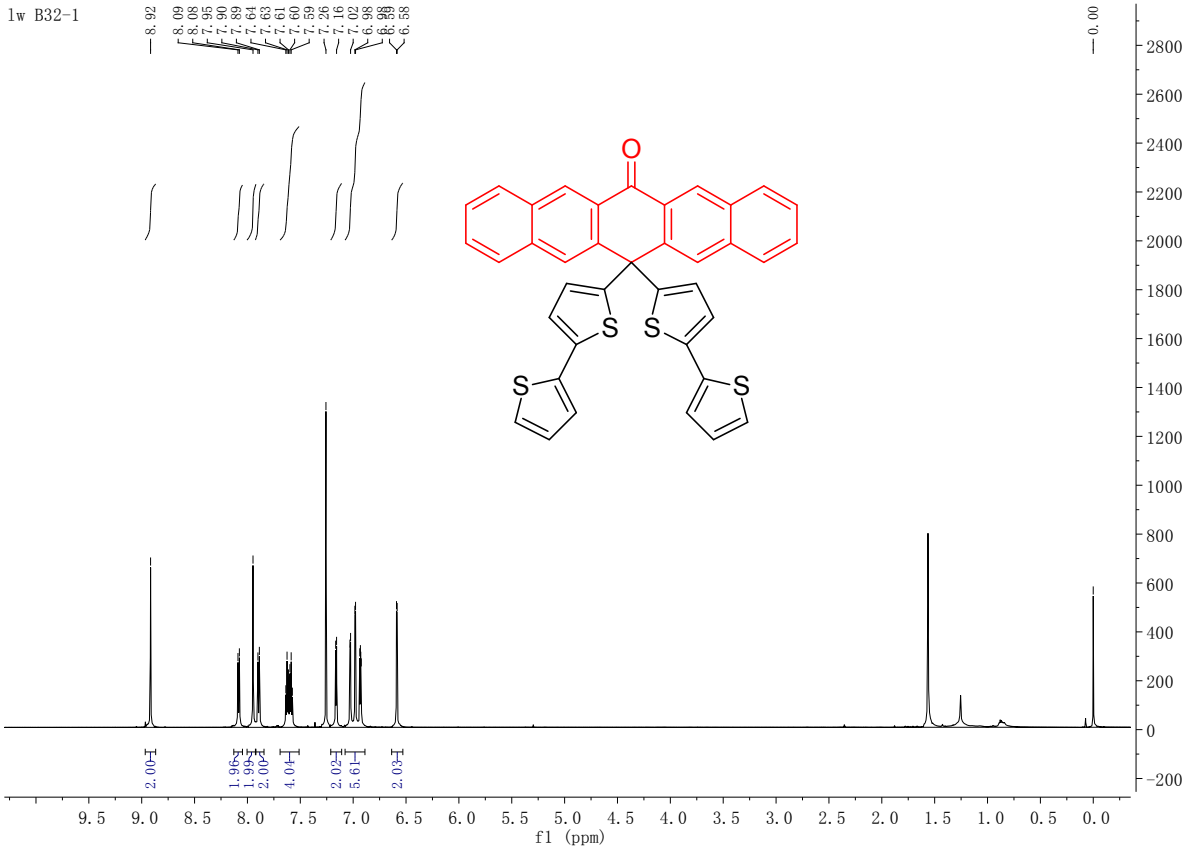
lw B32-1
8.92
8.09
8.08
7.95
7.90
7.89
7.64
7.63
7.61
7.60
7.59
7.26
7.16
7.02
6.98
6.58
0.00
2.00
1.96
1.99
2.00
4.04
2.02
5.61
2.03
O
S
S
S
S
f1 (ppm)

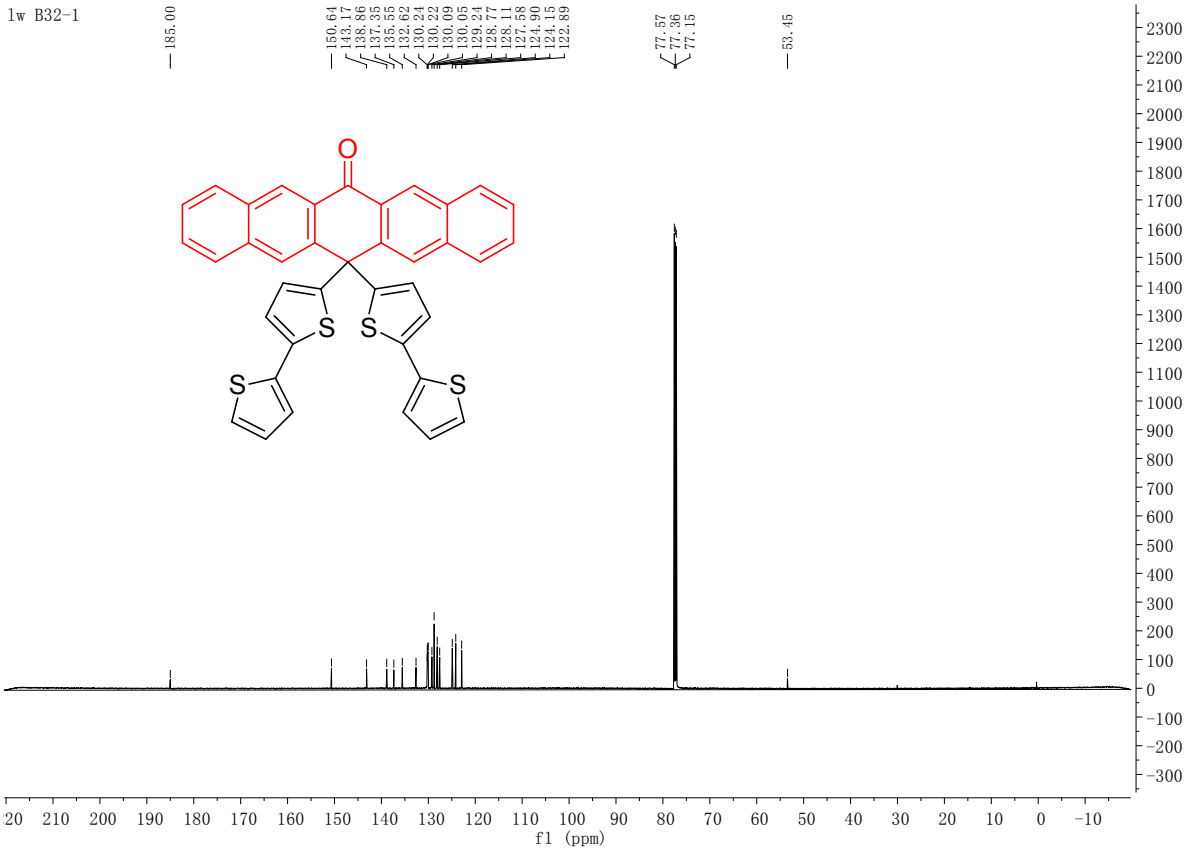
1w B32-1
185.00
150.64
143.17
138.86
137.35
135.55
132.62
130.24
130.22
130.09
130.05
129.24
128.77
128.11
127.58
124.90
124.15
122.89
77.57
77.36
77.15
53.45
O
S
S
S
S
f1 (ppm)

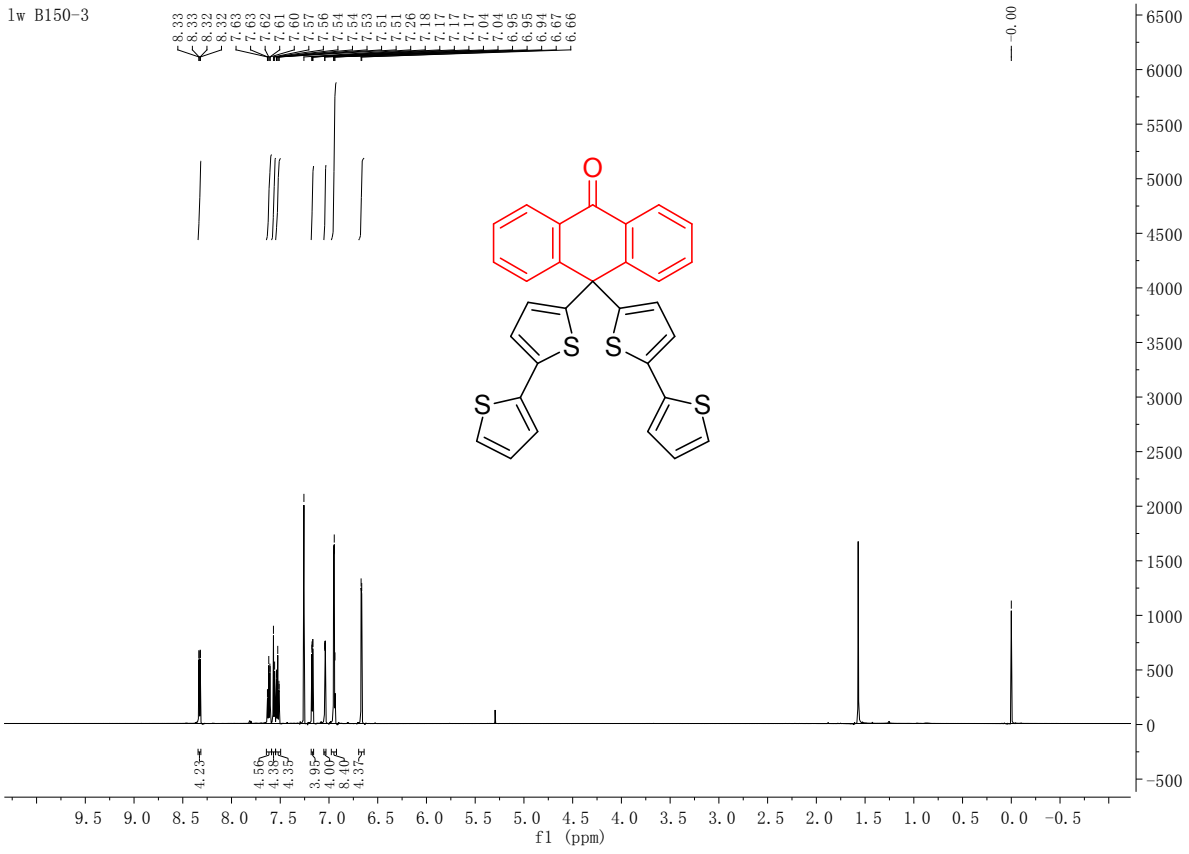
1w B150-3
8.33
8.33
8.32
8.32
7.63
7.62
7.61
7.60
7.57
7.56
7.54
7.54
7.53
7.51
7.51
7.26
7.18
7.17
7.17
7.17
7.04
7.04
6.95
6.95
6.94
6.67
6.66
-0.00
4.23
4.56
4.38
4.35
3.95
4.00
8.40
4.37
O
S
S
S
S
f1 (ppm)

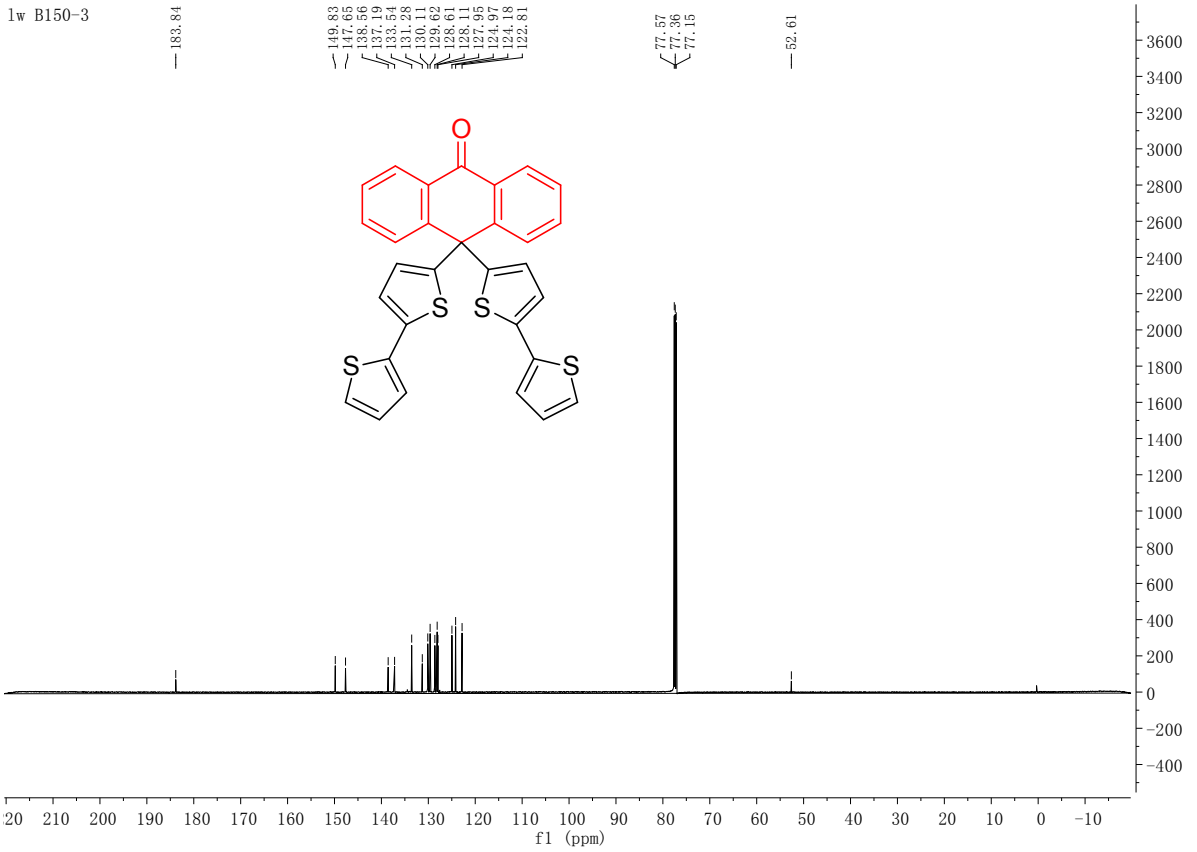
1w B150-3
183.84
149.83
147.65
138.56
137.19
133.54
131.28
130.11
129.62
128.61
128.11
127.95
124.97
124.18
122.81
77.57
77.36
77.15
52.61
O
S
S
S
S
f1 (ppm)

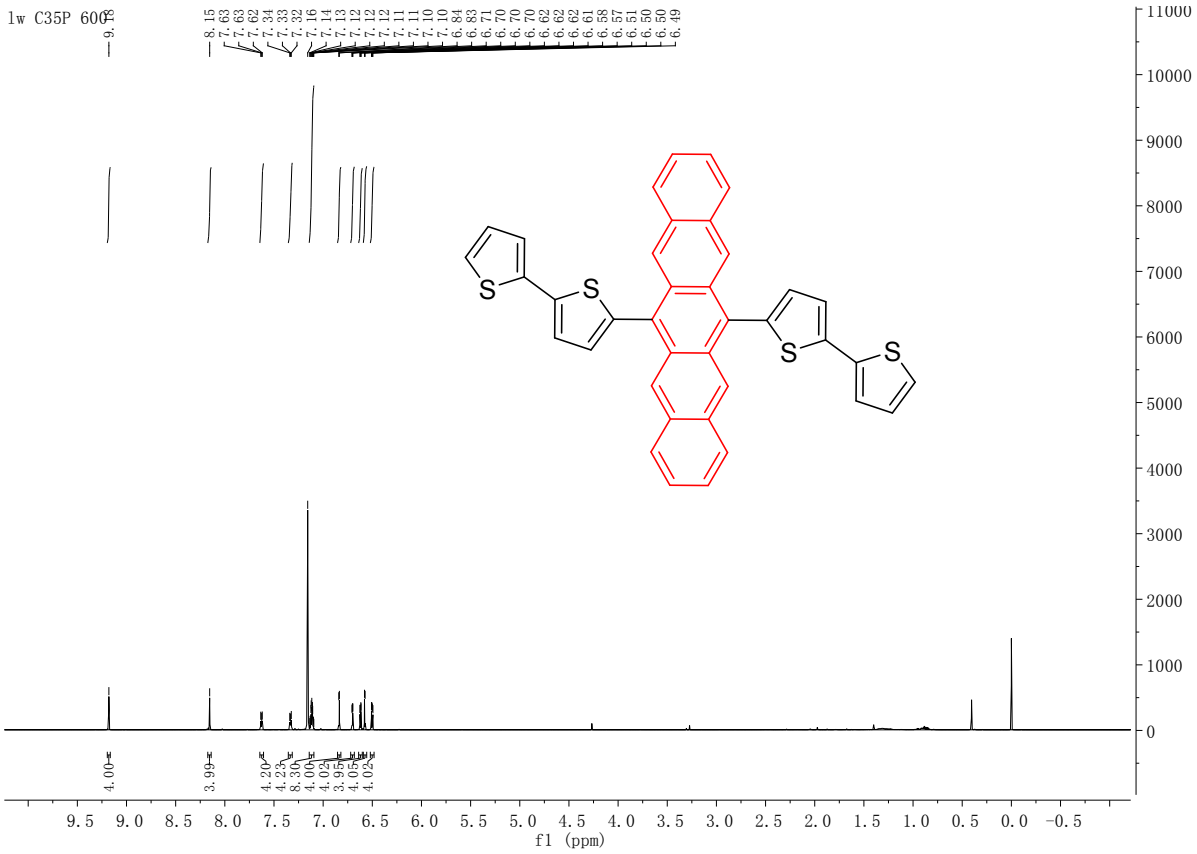
1w C35P 600
9.18
8.15
7.63
7.63
7.62
7.34
7.33
7.32
7.16
7.14
7.13
7.12
7.12
7.12
7.11
7.11
7.10
7.10
6.84
6.83
6.71
6.70
6.70
6.70
6.62
6.62
6.62
6.61
6.58
6.57
6.51
6.50
6.50
6.49
4.00
3.99
4.20
4.23
8.30
4.00
4.02
3.95
4.05
4.02
S
S
S
S
f1 (ppm)

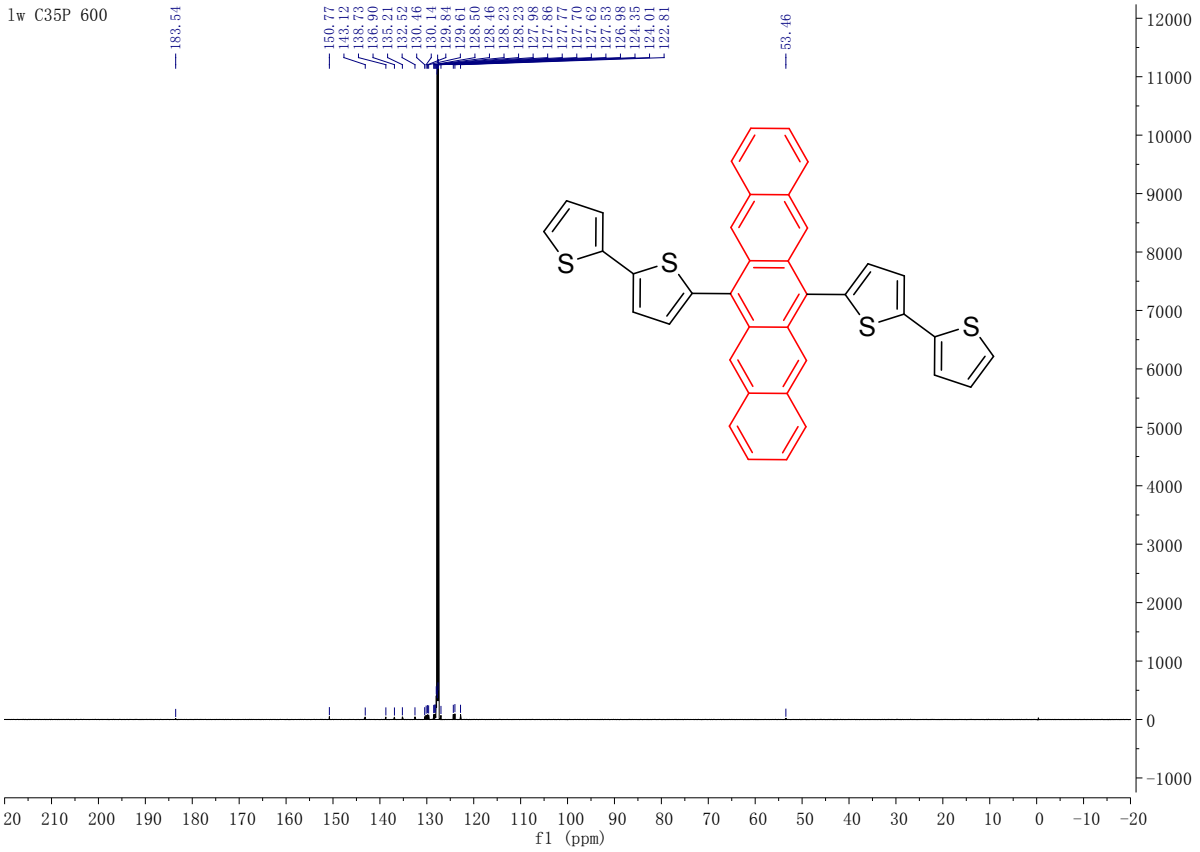
1w C35P 600
183.54
150.77
143.12
138.73
136.90
135.21
132.52
130.46
130.14
129.84
129.61
128.50
128.46
128.23
128.23
127.98
127.86
127.77
127.70
127.62
127.53
126.98
124.35
124.01
122.81
53.46
S
S
S
S
12000
11000
10000
9000
8000
7000
6000
5000
4000
3000
2000
1000
0
-1000
20 210 200 190 180 170 160 150 140 130 120 110 100 90 80 70 60 50 40 30 20 10 0 -10 -20
f1 (ppm)